

Sequential and Dendrite-Free Li Plating on Cu Foil Enabled by an Ultrathin Yolk–Shell SiO_x/C@C Layer

Ruhan He, Yutao Wang, Chengyi Zhang, Zhenhui Liu, Pan He, Xufeng Hong, Ruohan Yu, Yan Zhao, Jingsong Wu, Liang Zhou,* and Liqiang Mai*

Lithium metal anodes are considered to be the ultimate candidate for Li-based batteries; however, their development is hindered by uncontrollable Li deposition. Porous hosts and Cu foil with lithiophilic decorations have proven effective in Li dendrite suppression. However, the failure of lithiophilic decorations during cycling causes inaccessible encapsulated voids for Li-deposition. And the almost electrochemically inert feature of host/decoration materials will result in undesirable loss in gravimetric capacity. Herein, an ultrathin layer of stable and electroactive yolk-shell SiO_x/C@C with designed differences in lithiophilicity is constructed on Cu foil. The more lithiophilic SiO_x/C core over doped C shell induces sequential Li plating from intra-particle voids to inter-particle spaces and then above the modification layer. Such a plating process is reversed during Li stripping. Even after considering the mass of SiO_x/C@C modification layer, a high specific capacity of 2818 mAh g⁻¹ can be achieved. The Li–SiO_x/C@C–Cu anode demonstrates a decent cyclability over 500 h under strict conditions in symmetric cells. When paired with a LiFePO₄ cathode (10.5 mg cm⁻²), the full cell with a N/P ratio of 2 manifests a high capacity retention of 91.3% over 350 cycles, demonstrating its practical application value in future lithium metal batteries.

1. Introduction

Lithium metal anode with ultra-high specific capacity (3860 mAh g⁻¹) and extremely low redox potential (−3.040 V vs standard hydrogen electrode) is regarded as the “holy grail” for the high energy density storage systems. When paired with Ni-rich layered cathode materials (LiNi_xMn_yCo_zO₂), the lithium metal batteries (LMBs) are expected to reach an energy density of 500 Wh kg⁻¹.^[1–4] Considering the future application of sulfur (S) and oxygen (O₂) cathodes, the Li metal anode is even more indispensable. In spite of these advantages, its development has been severely hindered by the short lifetime and potential safety risks owing to the high chemical reactivity of traditional Li anodes.^[3,5,6] In addition, excessive Li is often used due to the poor processability of ultra-thin Li foil. The severe interface reactions and low utilization ratio have further reduced the specific capacities and aggravated the safety issues.^[1,7–9]

To tackle the above-mentioned problems of pure Li metal foil, researchers have pre-deposited Li metal with controllable thickness onto Cu foil.^[10] The Cu foil current collector, serving as the connection to external circuit and substrate for Li deposition, plays a decisive role in Li nucleation and growth. The uneven local electric field caused by the rough surfaces of the Cu foil leads to random Li nucleation. Due to the high nucleation overpotential of Li deposition on lithiophobic Cu, severe dendrite growth results (Scheme 1a). Thus, the modification of Cu foil, aiming at increasing Li affinity and reducing the variation of the local current density in charge, is crucial for improving the plating process.

Porous carbon materials with large surface areas are usually employed for Li hosts or Cu foil decoration, aiming to decrease the local current density and buffer the extremely large volume change of Li in the charge/discharge cycling.^[11–16] However, the interaction between pure carbon and Li is not strong enough; thus, lithiophilic species have to be introduced, for example, the loading of lithiophilic “sites” (Au, Ag, Zn) into inner surface of the hollow carbon can guide the deposition of Li into the hollow cavity.^[17–21] The aggregation or dissolution of these materials during cycling will lead to insufficient regulation effects and inaccessible voids for Li


R. He, Z. Liu, P. He, X. Hong, R. Yu, J. Wu, L. Zhou, L. Mai
State Key Laboratory of Advanced Technology
for Materials Synthesis and Processing
Wuhan University of Technology
Luoshi Road 122, Wuhan, Hubei 430070, China
E-mail: liangzhou@whut.edu.cn; mlq518@whut.edu.cn

R. He, R. Yu
International School of Materials Science and Engineering
Wuhan University of Technology
Wuhan, Hubei 430070, China

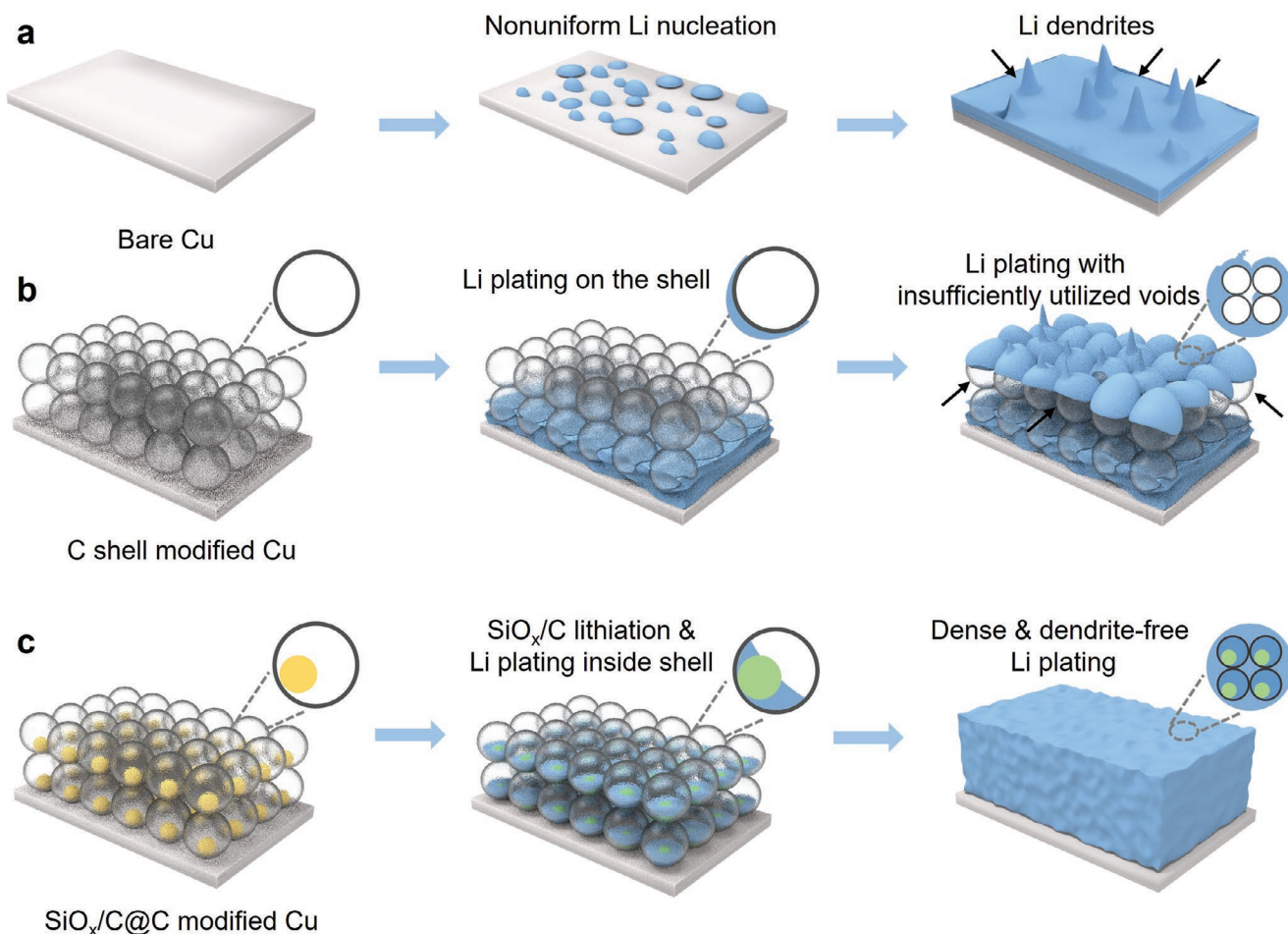
Y. Wang, R. Yu, J. Wu
Nanostructure Research Centre
Wuhan University of Technology
Luoshi Road 122, Wuhan, Hubei 430070, China

C. Zhang, Y. Zhao
Institute of Technological Sciences
Wuhan University
Wuhan, Hubei 430072, China

L. Zhou, L. Mai
Hubei Longzhong Laboratory
Wuhan University of Technology (Xiangyang Demonstration Zone)
Xiangyang, Hubei 441000, China

 The ORCID identification number(s) for the author(s) of this article can be found under <https://doi.org/10.1002/aenm.202204075>.

DOI: 10.1002/aenm.202204075



Scheme 1. Scheme illustration for the Li plating behaviours on a) bare Cu foil, b) C shell modified Cu foil, and c) SiO_x/C@C modified Cu foil.

deposition. Besides, some oxide-based lithiophilic “sites” (TiO₂, SiO_x/C) have also been employed to regulate the Li deposition, demonstrating better structural stability than the above-mentioned metallic lithiophilic “sites.”^[22,23] Doping the carbon materials with foreign atoms can also improve the lithiophilicity;^[24–26] however, as Li is deposited only on the surface of the hollow carbon without entering it,^[27] Li dendrites will form as well when the deposited Li increases (Scheme 1b). Due to the insufficiently utilized void space, the Li storage capacities are usually low (<3 mAh cm⁻²) before the dendrite is formed. In addition, a thick decoration layer is needed if a large Li loading amount (5 mAh cm⁻²) is required, and the benefits of high specific capacity for Li metal have been compromised.^[4,28] Thus, to build an effective decoration layer, it is necessary to expand the available Li storage space and reduce its weight ratio in the electrode, as well as maintain effective regulation toward Li deposition.

Herein, we design a yolk–shell SiO_x/C@N/S-doped C (SiO_x/C@C) architecture with a highly lithiophilic SiO_x-based core and carbon-based shell. The difference in Li affinity induces a sequential and homogenous Li-plating process on decorated Cu foil (Scheme 1c). The SiO_x/C cores with high affinity toward Li are lithiated first, serve as the “seeds,” and guide the Li to preferentially deposit into the cavity between the SiO_x/C

core and C shell. The N/S co-doped C shells not only enable a uniform local electrical field but also serve as the secondary lithiophilic sites and lead to the dense Li plating in the interparticle voids. The continuous conductive path and uniform current field enable a homogeneous and dense Li layer deposited above the modification layer. In result, the sequential plating behavior affords the Li metal anode with a high specific gravimetric (volumetric) capacity of 2818 mAh g⁻¹ (1250 mAh cm⁻³). It achieves a stable cycling for 400 cycles with 1 mAh cm⁻² Li and high average CE of 98.8% with 5 mAh cm⁻² Li. When paired with a LiFePO₄ cathode with a high mass loading of 10.5 mg cm⁻², the full cell with a N/P ratio of 2 can be cycled for 350 cycles without obvious capacity fading.

2. Results and Discussion

The SiO_x/C@C spheres are prepared through a sol–gel method using vinyltrimethoxysilane derived organosilica as the sacrificial layer (Figure S1, Supporting Information).^[29,30] Scanning electron microscopy (SEM) and transmission electron microscopy (TEM) characterizations show the SiO_x/C@C sphere possesses a diameter of ≈500 nm, which is composed of a solid SiO_x/C core with a size of ≈250 nm and a N/S co-doped

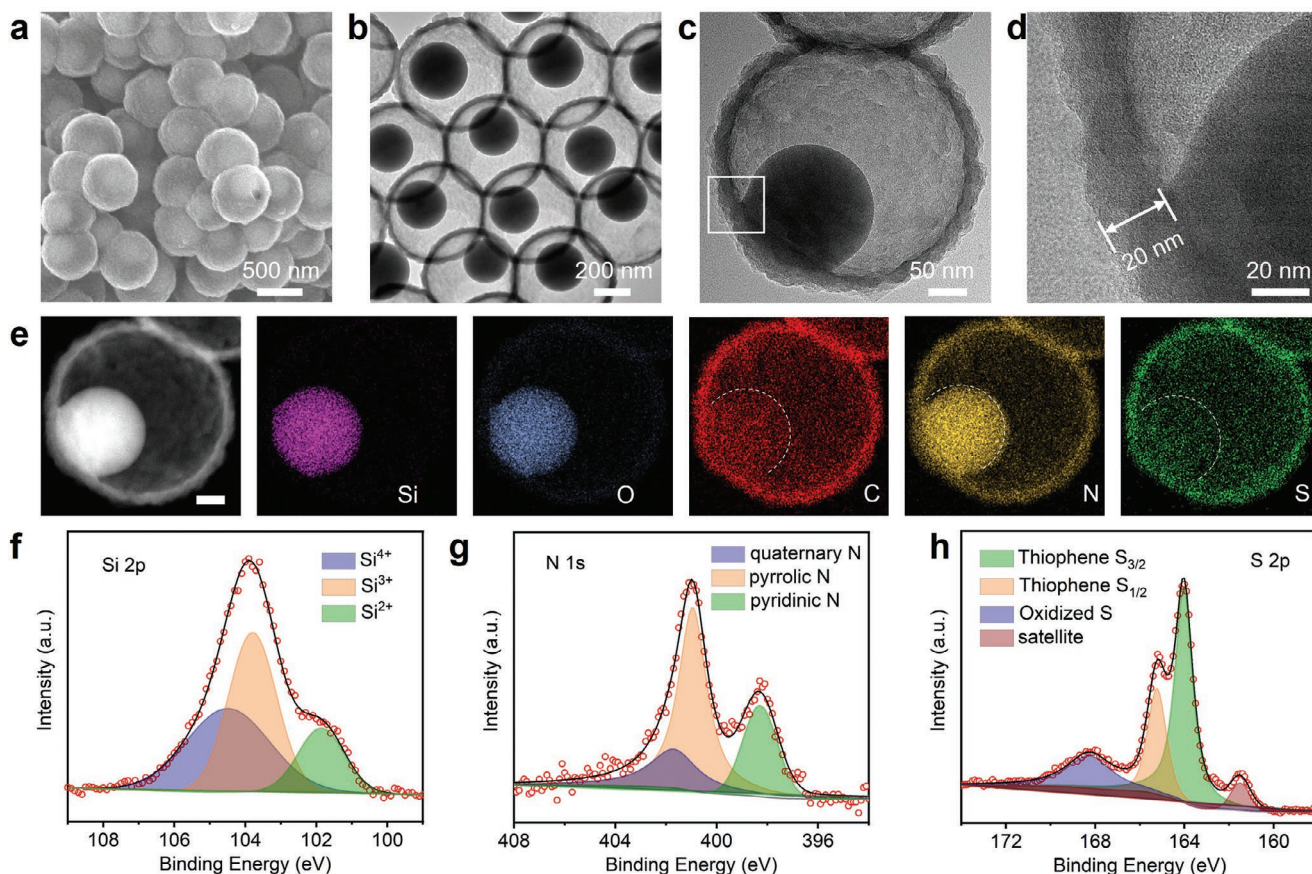


Figure 1. a) SEM image, b–d) TEM images, e) HAADF-STEM and EDS elemental mapping (scale bar: 50 nm), f) Si2p, g) N1s, and h) S2p high-resolution XPS spectra of SiO_x/C@C yolk-shell spheres.

hollow C shell with a thickness of ≈ 20 nm (Figure 1a–d). The high angle annular dark field scanning transmission electron microscopy (HAADF-STEM) and the corresponding energy dispersive spectrometry (EDS) elemental mapping show a uniform distribution of Si and O elements in the core and C, N, and S signals throughout the yolk-shell structure (Figure 1e). The S is originated from the $-\text{SCN}$ group of the 3-thiocyanatopropyltriethoxysilane (TCPTES, the precursor for the yolk), and the doping of S in the carbon shell is caused by the escape of S-containing small molecules from the yolk during high-temperature treatment.

X-ray diffraction (XRD, Figure S2, Supporting Information) pattern shows the amorphous state of SiO_x/C@C and the Si2p X-ray photoelectron spectroscopy (XPS, Figure 1f) spectrum indicates that the average valence of Si is ≈ 3.1 .^[23,31,32] The successful doping of N and S in C shell is confirmed by the XPS survey spectrum (Figure S3, Supporting Information), N1s spectrum (Figure 1g), and S2p spectrum (Figure 1h). The N1s spectrum is deconvoluted into three peaks, corresponding to the quaternary N (401.7 eV), pyrrolic N (401.0 eV), and pyridinic N (398.3 eV) peaks.^[33] The S2p spectrum is deconvoluted into four peaks, namely the S_{1/2} (165.2 eV) and S_{3/2} (164.0 eV) components of thiophene, oxidized S (168.2 eV), and the satellite (161.5 eV).^[34] As is shown in Table S1, Supporting Information, the N and S element content of SiO_x/C@C yolk-shell spheres are 3.88%

and 1.16%, respectively. The doping of N and S elements in carbon is beneficial to the conductivity and lithiophilicity.^[34,35] The SiO_x/C@C presents a high specific surface area of 276.3 m² g⁻¹, indicating the porous structure of the exterior C shell, which is beneficial for Li⁺ diffusion (Figure S4, Supporting Information).^[36] For comparison, the SEM, TEM, and XPS characterizations of hollow C shells are shown in Figures S5 and S6a, Supporting Information. XPS survey spectra of SiO_x/C solid sphere shows both S2p and N1s signals (Figure S6b, Supporting Information) and TCPTES is the only S-containing precursor that participates in the preparation process of SiO_x/C@C. Thus, it is rational to deduce that the doped S atoms in the C shell come from the thiocyanate groups ($-\text{SCN}$) due to the escape of S-containing small molecules from the inner cores during heat treatment.

When coated onto Cu foil, the SiO_x/C@C spheres and C shells are well assembled into a continuous film with smooth surface, which is beneficial for the homogenous Li deposition (Figure S7, Supporting Information). The average thickness of the modification layer is ≈ 8 μm . As the dendrite-free Li plating is a prerequisite for Li metal anode with high performance, we examine the morphology of Cu foil, C shell modified Cu foil, and SiO_x/C@C modified Cu foil after the deposition of 5 mAh cm⁻² Li at 1 mA cm⁻². After Li deposition, the bare Cu foil is fully covered with mossy Li (Figure 2a,b). The mossy Li disorderly grows into Li dendrites after ten cycles (Figure S8a,b,

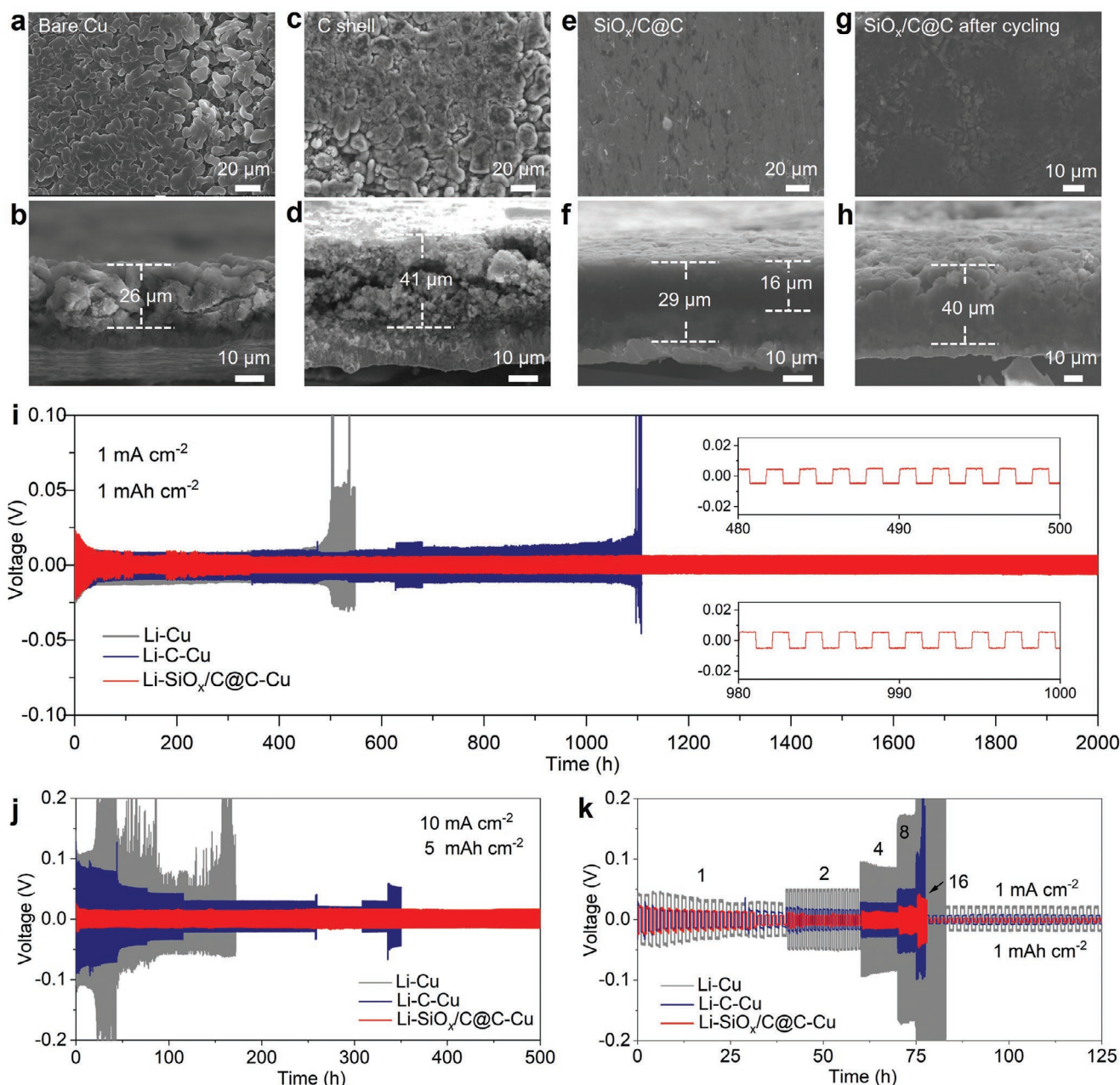


Figure 2. Plane view and cross-sectional view SEM images of Li deposited (5 mA h cm^{-2}) on a,b) bare Cu, c,d) C shell modified Cu foil at the 1st cycle. g,h) SEM images of Li deposited (5 mAh cm^{-2}) on SiO_x/C@C modified Cu after ten cycles. Galvanostatic cycling of a Li||Li-SiO_x/C@C-Cu (red), Li||Li-C-Cu (blue), and Li||Li-Cu (gray) under i) $1 \text{ mA cm}^{-2}/1 \text{ mAh cm}^{-2}$, j) $10 \text{ mA cm}^{-2}/5 \text{ mAh cm}^{-2}$, and k) 1, 2, 4, 8, 16 $\text{mA cm}^{-2}/1 \text{ mAh cm}^{-2}$.

Supporting Information), accompanied by an increase in electrode thickness. The Li metal deposited on C shell modified Cu foil also shows visible Li dendrites (Figure 2c,d; Figure S8c, Supporting Information). After cycling, the electrode thickness is largely increased from 41 to 64 μm, showing a rather fluffy cross section (Figure S8d, Supporting Information). On the contrary, the SiO_x/C@C electrode after Li deposition exhibits a dense and smooth surface pattern with an initial thickness of ≈30 μm (including the thickness of modification layer), which is only 5 μm thicker than the pure Li foil with a capacity of

5 mAh cm^{-2} . No obvious Li dendrite is observed from either plane view or cross-sectional view (Figure 2e,f). It is interesting that the Li-SiO_x/C@C-Cu electrode shows three different layers as can be told from the contrast difference in Figure 2f. The corresponding EDS elemental mapping shows that O, Si, and Cu elements are enriched in the top, middle, and bottom layers, respectively (Figure S9, Supporting Information). The enrichment of O on the top layer is possibly from the oxidation of metallic Li to Li₂O during sample preparation. Thus, we deduce that a pristine Li layer is deposited above the SiO_x/C@C

decoration layer. After ten cycles, the dendrite-free characteristic of Li-SiO_x/C@C-Cu electrode is well maintained, with a moderate thickness expansion (Figure 2g,h). The above results indicate that the SiO_x/C@C decoration on Cu foil successfully induces the homogenous deposition of Li even after Li plating/stripping cycles.

To evaluate the effects of SiO_x/C@C modification layer on long-term cycling, symmetric cells are assembled with pre-deposited Li electrodes (Li-Cu, Li-C-Cu and Li-SiO_x/C@C-Cu). Comparing with the Li-Cu and Li-C-Cu electrodes, the Li-SiO_x/C@C-Cu shows much lower polarizations, either in mild testing conditions (10 mV at 1 mA cm⁻²/1 mAh cm⁻²) or in strict testing conditions (16 mV at 10 mA cm⁻²/5 mAh cm⁻²). Under the condition of 1 mA cm⁻²/1 mAh cm⁻², the low polarization can be well maintained for 2000 h without distinct fluctuation (Figure 2i). However, the polarization of Li-Cu electrode increases dramatically after 500 h under this mild plating/stripping conditions. Even at a high current density of 10 mA cm⁻² and high Li loading amount of 5 mAh cm⁻², the Li-SiO_x/C@C-Cu anode still demonstrates an excellent stability (500 h) with a slight increase in voltage (Figure 2j). The Li-SiO_x/C@C-Cu based symmetric cell can be stably cycled at current densities varying from 1 to 16 mA cm⁻², and the voltage hysteresis are

much lower comparing to the other two cells (Figure 2k). Especially, the Li-SiO_x/C@C-Cu based cell maintains a small and steady voltage variation of 40 mV even at a high current density of 16 mA cm⁻². In contrast, the Li-Cu and Li-C-Cu based cells show drastically rising polarizations under the same conditions. The above results demonstrate that the Li-SiO_x/C@C-Cu electrode possesses high stability for long-term cycling even at high current density, proving its potential application under practical testing conditions.

In situ TEM is conducted to reveal the Li deposition behavior in the yolk-shell SiO_x/C@C. The nanosized dry cell in TEM equipment is constructed by connecting the single SiO_x/C@C sphere with the Li₂O on the surface of Li metal attached on the tungsten tip.^[37] As soon as a biased voltage is applied, the electrochemical process is triggered in the nano half-cell battery. Video S1, Supporting Information; selected snapshots (Figure 3a) vividly exhibit the lithium storage process in the SiO_x/C@C. Specifically, the SiO_x/C core first experiences the lithiation process with a moderate but visible volume expansion (529s).^[38] Shortly after (565s), Li starts to deposit in the void of SiO_x/C@C and rapidly takes up one third of the void space. The filling process is proceeding with the movement of the boundary between unfilled and filled areas. At ≈891 s, the Li overspreads all

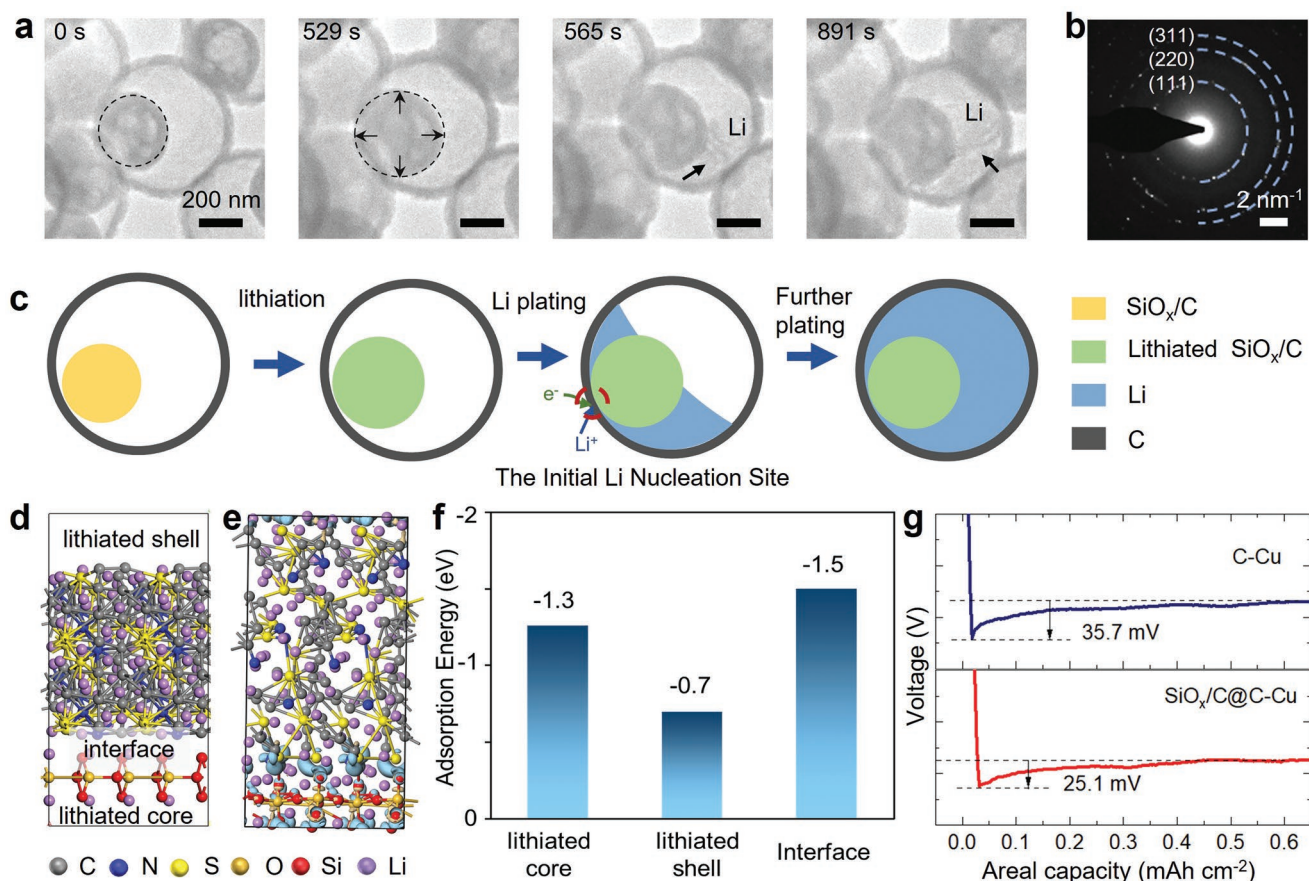


Figure 3. a) Selected TEM snapshots showing the lithiation/Li plating process of yolk-shell SiO_x/C@C; b) selected area electron diffraction pattern; c) schematic illustration showing the lithiation/Li plating of SiO_x/C@C; d) molecular models of the lithiated core and shell before optimization; e) molecular models of the lithiated core, lithiated shell, and interface after optimization with the charge density difference map; f) adsorption energy toward Li from different active sites; and g) Li deposition overpotential on C shell and SiO_x/C@C modified Cu foil.

the void, as evidenced by the visualized wrinkled texture (indicated by the black arrows) and obvious diffraction rings from Li_2O in Figure 3b. Besides, a broad peak (55 eV) corresponding to the *K*-edge of Li metal is captured in electron energy-loss spectroscopy (EELS) spectra, confirming the successful Li deposition into the interior space of the $\text{SiO}_x/\text{C}@C$ (Figure S10, Supporting Information).^[39] It is worth noting that even if all the neighboring spheres are fully filled, there is no Li dendrite growth on the surface of $\text{SiO}_x/\text{C}@C$ (Video S1, Supporting Information), which is often observed on bare C shells.^[27,40,41] The dendrite-free Li deposition in the void of $\text{SiO}_x/\text{C}@C$ should be largely attributed to the superior Li affinity of SiO_x/C core. Meanwhile, the spherical morphology of $\text{SiO}_x/\text{C}@C$ is well maintained after cycling, without dissolution or aggregation problems such as lithiophilic Au or Ag “seeds” (Figure S11, Supporting Information).^[22,42] Reviewing the whole lithiation/Li plating process of yolk-shell $\text{SiO}_x/\text{C}@C$ as shown in Video S1, Supporting Information; Figure 3a, it is observed that the Li deposition always begins at the interface, that is to say, the contact point between SiO_x/C core and N,S co-doped C shell (indicated by the red circle in Figure 3c).

Density functional theory (DFT) simulation is employed to clarify the superior Li deposition behavior on $\text{SiO}_x/\text{C}@C$ modified Cu over bare Cu and C shell modified Cu. The molecular models of lithiated SiO_x/C core and N/S-doped C shell are constructed (Figure S12, Supporting Information; Figure 3d). After

the optimization of molecular model (Figure 3e), new bonds between core and shell are formed with a large amount of charge transfer, which indicates a distinct change of the chemical environment at the interface. This in turn results in a more negative adsorption energy (−1.5 eV) at the interface than both core (−1.3 eV) and shell (−0.7 eV). The more negative adsorption energy means the higher affinity to Li, which explains why the Li deposition begins at the interface (Figure 3f). The higher affinity toward Li would enable a lower Li nucleation barrier, which can also be reflected in the nucleation overpotential. As shown in Figure 3g; Figure S13, Supporting Information, the Li deposition overpotential on $\text{SiO}_x/\text{C}@C$ (25.1 mV) is lower than that on C shell (35.7 mV), which is consistent with the results on adsorption energy. Thus, it is the highly lithiophilic interface formed between core and shell that successfully induces Li^+ to overcome the heterogeneous nucleation barrier and deposit in the interior space of $\text{SiO}_x/\text{C}@C$.

The Li plating/stripping behaviors on $\text{SiO}_x/\text{C}@C$ modified Cu foil are investigated with the help of focused ion beam (FIB) technique. The initial thickness of $\text{SiO}_x/\text{C}@C$ layer is measured to be 6 μm (Figure 4a). When 1 mAh cm^{-2} Li is deposited, the decoration layer swells up to 10 μm (Figure 4b). The FIB cut $\text{SiO}_x/\text{C}@C$ electrode shows that the initial intra-particle voids become partially solid, which is caused by the deposition of Li metal (Figure S14, Supporting Information). On the contrary, the voids of C shells remain largely unoccupied and the Li

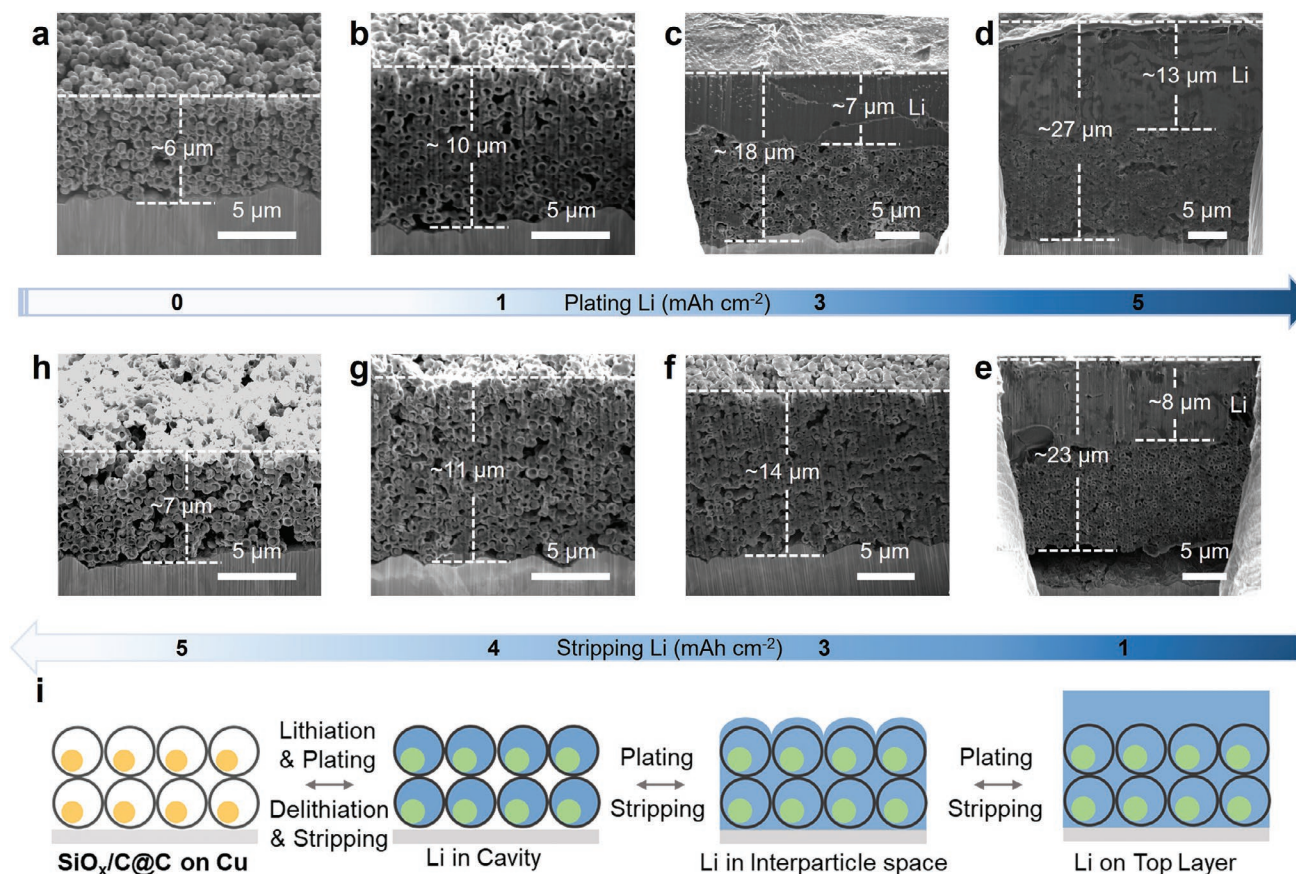


Figure 4. FIB assisted cross-sectional SEM images of $\text{SiO}_x/\text{C}@C$ decorated Cu foil a) without Li deposition; b–d) with Li plating amounts of 1, 3, and 5 mAh cm^{-2} ; and e–h) with Li stripping amounts of 1, 3, 4, to 5 mAh cm^{-2} ; i) schematic illustration of the sequential Li plating/stripping process.

metal tends to deposit in the inter-particle voids as well as on top of the decoration layer (Figure S15, Supporting Information). With the Li amount increased to 3 mAh cm⁻², the thickness of Li-SiO_x/C@C layer increases to 18 μm (Figure 4c). At this stage, Li metal has taken up the inter-particle spaces. Meanwhile, a layer of Li metal can be observed on the top of the electrode. When the deposited Li amount reaches 5 mAh cm⁻², the cross-sectional SEM image clearly shows the layered structure of Li-SiO_x/C@C-Cu electrode, with a dense Li layer (≈13 μm) on the top, a decoration layer (≈14 μm) in the middle, and the Cu foil at the bottom (Figure 4d). These observations are highly consistent with the results in Figure 2f, strongly proving the sequential Li deposition behavior on SiO_x/C@C decorated Cu foil. The slight difference in the electrode thickness measured through two techniques (Figures 2f and 4d, respectively) are caused by variation of the thickness of decoration layer from different batches of electrodes.

Figure 4e-h shows the corresponding sequential stripping process, with the Li stepwise stripped away from the top layer (Figure 4e), the inter-particle space (Figure 4f), and then the interior space of SiO_x/C@C (Figure 4g). The SiO_x/C@C decoration layer is nearly recovered to its original shape after the stripping process; although, a slight swelling is observed (Figure 4h). In conclusion, the Li plating/stripping process is proved to be sequential and highly reversible on SiO_x/C@C decorated Cu foil (Figure 4i). Even if the interaction between the top Li metal layer

and the decoration layer gradually weakens as the Li amount increases, the whole Li-SiO_x/C@C electrode can well maintain the dendrite-free pattern. When loaded with 5 mAh cm⁻² Li, the Li-SiO_x/C@C layer shows a thickness of ≈27 μm, slightly thicker than the pristine Li (5 mAh cm⁻², 25 μm). Even after considering the mass (thickness) of SiO_x/C@C modification layer, a high gravimetric (volumetric) capacity of ≈2818 mAh g⁻¹ (≈1250 mAh cm⁻³) can be achieved (The thickness of Li-SiO_x/C@C layer is calculated with the value of 30 μm according to Figure 2f). Comparing to decoration layers/host materials with dozens or even hundreds of micrometers, the thinner SiO_x/C@C layer not only realizes a dendrite-free Li anode but also avoids the sacrificing of high capacity.

The Coulombic efficiency (CE), which is an important parameter to evaluate the cycle lifetime of Li metal anode, is shown in Figure 5a,b; Figure S16, Supporting Information. The Li-SiO_x/C@C-Cu electrode processes a high initial Coulombic efficiency (ICE) of 95.5% and an average CE value of 98.5% during a long-term cycling (400 cycles). The discharge/charge curves of Li-SiO_x/C@C-Cu show low Li growth overpotential (10 mV) without distinct fluctuations (Figure S17a, Supporting Information), further indicating its high cycling stability. The Li-Cu electrode experiences a quick fail at around the 50th cycle, with a relatively low ICE of 92.2%. As for the Li-C-Cu, it shows a higher ICE (93.5%) and longer cycling life than Li-Cu, but the CE still undergoes a distinct drop in no more

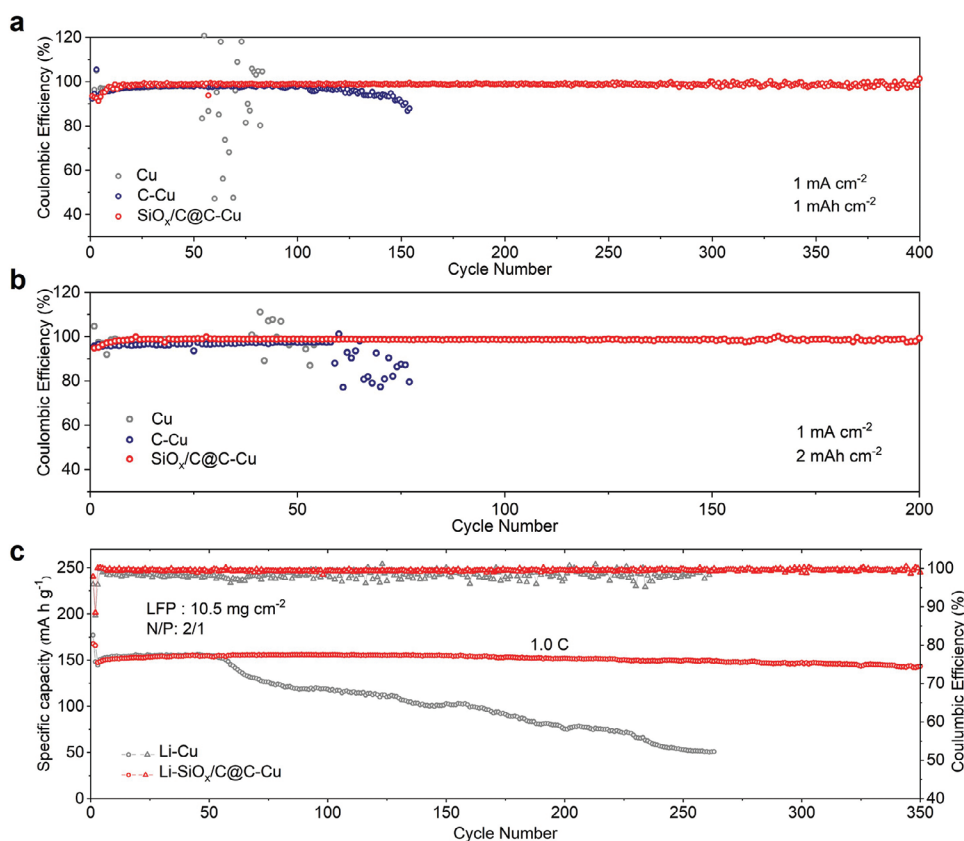


Figure 5. CE tests of a Li||SiO_x/C@C-Cu (red), Li||C-Cu (blue), and Li||Cu (gray) at the current density of 1.0 mA cm⁻² and Li deposition amount of a) 1.0 mAh cm⁻², b) 2.0 mAh cm⁻², and c) cycling performances of the Li-Cu||LFP and Li-SiO_x/C@C-Cu||LFP full cells at charging/discharging rates of 1 C (1 C = 170 mAh g⁻¹).

than 100 cycles. The average CE of Li–C–Cu half-cell is 97.6% for 100 cycles, lower than that of Li–SiO_x/C@C–Cu half-cells (98.5%, 400 cycles). The relatively high Li growth overpotential (18 mV) and random fluctuations in discharge/charge curves at 170 cycles indicate its unsatisfactory cycling stability (Figure S17b, Supporting Information). When the Li amounts are increased to 2 and 5 mAh cm⁻², the Li–SiO_x/C@C–Cu shows average CEs of 98.6% and 98.8%, respectively, outperforming the other two electrodes. Besides, the Li–SiO_x/C@C–Cu also shows the lowest interfacial impedance after cycling, demonstrating its ideal interfacial stability (Figure S18, Supporting Information). The CE of SiO₂ modified Cu has also been tested, and the poor conductivity and low electrochemical activity of SiO₂ will lead to a poor cycling stability with decreased capacity (Figure S19, Supporting Information). When compared to Cu substrate modified with different materials reported recently, such as lithiophilic sites, hollow carbon spheres, lithiophilic sites decorated carbon materials and so on, the SiO_x/C@C–Cu shows advantages in specific capacity and cycling stability (Table S2, Supporting Information).

To verify the feasibility of SiO_x/C@C modification layer for practical application, full cells are assembled with lithium iron phosphate (LFP) as the cathode. Here, the LFP loading is ≈10.5 mg cm⁻² (≈1.5 mAh cm⁻²) and the N/P ratio is 2. The full cell with Li–SiO_x/C@C–Cu anode exhibits a specific capacity of 140 mAh g⁻¹ after 350 cycles at 1 C, with a high capacity retention of 91.3% (Figure 5c). In contrast, the counterpart with Li–Cu anode experiences a quick capacity drop after 50 cycles, with only 50% capacity retention after 200 cycles. The charge/discharge voltage profiles of full cell with Li–SiO_x/C@C–Cu anode (Figure S20a, Supporting Information) also show a lower polarization than that with Li–Cu anode, indicating a more stable electrode–electrolyte interface. Rate performances of the Li–SiO_x/C@C–Cu||LFP full cell are exhibited in Figure S20b, Supporting Information, and the cell delivers a high specific capacity of 113 mAh g⁻¹ at 4 C. The N/P ratio is further decreased to 1.1/1; the cycling performances of Li–SiO_x/C@C–Cu||LFP full cell also outperforms the Li–Cu||LFP full cell, showing a specific capacity of ≈100 mAh g⁻¹ after 200 cycles (Figure S21, Supporting Information). It is concluded that the superior Li deposition behavior regulated by the SiO_x/C@C modification layer can also play a positive effect in full cells. From Table S3, Supporting Information, we could tell that the full cell performance of SiO_x/C@C modification layer modified anode shows superior cycling performance when compared to other hollow carbon structure-modified electrodes.

3. Conclusion

To conclude, yolk–shell structured SiO_x/C@C consisting of a highly lithiophilic SiO_x/C core and less lithiophilic N/S-doped C shell has been successfully designed to regulate Li deposition. Benefiting from the lithiophilic differences between SiO_x/C core and N/S-doped C shell, the SiO_x/C@C modified Cu foil demonstrates a sequential and dendrite-free Li plating/stripping behavior. The more lithiophilic SiO_x/C core acts as the primary “seed” for Li deposition and guides the deposition of Li in the intra-particle void through the C shell. The N/S

doped C shell acts as the secondary lithiophilic “seed,” inducing the deposition of Li in the inter-particle voids. After filling the intra-particle and inter-particle voids, the Li starts to plate on the top of the decoration layer, forming a homogeneous and compact layer. Benefiting from the stepwise and homogeneous Li deposition, the Li–SiO_x/C@C–Cu electrode achieves a high CE over 98.5% over 400 cycles. A low polarization of 10 mV can be well maintained after 2000 h plating/stripping processes in symmetric cells. When coupled with a high mass loading (10.5 mg cm⁻²) LFP cathode, the full cell with a N/P ratio of 2 can be cycled for 350 cycles without obvious capacity fading. The design of hetero-structured materials with regulated lithiophilic sites may inspire the further construction of functional current collectors for Li deposition; and thus, promote the development of advanced Li metal anode and Li metal batteries.

Supporting Information

Supporting Information is available from the Wiley Online Library or from the author.

Acknowledgements

This work was supported by the National Key Research and Development Program of China (Grant No. 2020YFA0715000), the National Natural Science Foundation of China (Grant No. 52127816, 52072282), the Key Research and Development Program of Hubei Province (2021BAA176), the Hainan Provincial Natural Science Foundation of China (522CXTD516), and the Natural Science Foundation of Jiangsu Province (Grant No. BK20220912).

Conflict of Interest

The authors declare no conflict of interest.

Author Contributions

R.H., Y.W., and C.Z. contributed equally to this work. R.H., Z.L., and L.Z. conceived the idea. R.H. designed, conducted the experiments, and wrote the manuscript. Y.W. and R.Y. assisted in the in situ TEM experiments; C.Z. assisted in the calculation parts. P.H., X.H., Y.Z., J.W., and L.Z. assisted in the revision of the manuscript. L.Z. and L.M. supervised the whole project. All authors discussed the results and commented on the manuscript.

Data Availability Statement

The data that support the findings of this study are available from the corresponding author upon reasonable request.

Keywords

lithiophilic sites, lithium metal batteries, metal anodes, silicon-based materials, yolk–shell structures

Received: November 29, 2022

Revised: February 19, 2023

Published online:

- [1] D. Lin, Y. Liu, Y. Cui, *Nat. Nanotechnol.* **2017**, *12*, 194.
- [2] F. Wu, J. Maier, Y. Yu, *Chem. Soc. Rev.* **2020**, *49*, 1569.
- [3] X. Shen, H. Liu, X. B. Cheng, C. Yan, J. Q. Huang, *Energy Storage Mater.* **2018**, *12*, 161.
- [4] S. Kim, G. Park, S. J. Lee, S. Seo, K. Ryu, C. H. Kim, J. W. Choi, *Adv. Mater.* **2022**, *n/a*, 2206625.
- [5] X. B. Cheng, R. Zhang, C. Z. Zhao, Q. Zhang, *Chem. Rev.* **2017**, *117*, 10403.
- [6] X. Zhang, Y. Yang, Z. Zhou, *Chem. Soc. Rev.* **2020**, *49*, 3040.
- [7] R. Xu, X.-B. Cheng, C. Yan, X. Q. Zhang, Y. Xiao, C. Z. Zhao, J. Q. Huang, Q. Zhang, *Matter* **2019**, *1*, 317.
- [8] Y. Zhang, T. T. Zuo, J. Popovic, K. Lim, Y. X. Yin, J. Maier, Y. G. Guo, *Mater. Today* **2020**, *33*, 56.
- [9] S. Tan, Y. Jiang, S. Ni, H. Wang, F. Xiong, L. Cui, X. Pan, C. Tang, Y. Rong, Q. An, *Natl. Sci. Rev.* **2022**, *9*, nwac183.
- [10] B. Zhou, A. Bonakdarpour, I. Stoševski, B. Fang, D. P. Wilkinson, *Prog. Mater. Sci.* **2022**, *130*, 100996.
- [11] H. Ye, S. Xin, Y. X. Yin, J. Y. Li, Y. G. Guo, L. J. Wan, *J. Am. Chem. Soc.* **2017**, *139*, 5916.
- [12] Z. Liang, D. Lin, J. Zhao, Z. Lu, Y. Liu, C. Liu, Y. Lu, H. Wang, K. Yan, X. Tao, Y. Cui, *Proc. Natl. Acad. Sci. U. S. A.* **2016**, *113*, 2862.
- [13] H. Ye, S. Xin, Y.-X. Yin, Y.-G. Guo, *Adv. Energy Mater.* **2017**, *7*, 1700530.
- [14] S. Park, H.-J. Jin, Y. S. Yun, *Adv. Mater.* **2020**, *32*, 2002193.
- [15] H. Yuan, J. Nai, H. Tian, Z. Ju, W. Zhang, Y. Liu, X. Tao, X. W. Lou, *Sci. Adv.* **2020**, *6*, eaaz3112.
- [16] Y. Fang, S. L. Zhang, Z. P. Wu, D. Luan, X. W. Lou, *Sci. Adv.* **2021**, *7*, eabg3626.
- [17] D. Fang, Y. Wang, X. Liu, J. Yu, C. Qian, S. Chen, X. Wang, S. Zhang, *ACS Nano* **2019**, *13*, 1563.
- [18] Z. T. Wondimkun, W. A. Tegege, J. Shi Kai, C. J. Huang, N. A. Sahalie, M. A. Weret, J. Y. Hsu, P. L. Hsieh, Y. S. Huang, S. H. Wu, W. N. Su, B. J. Hwang, *Energy Storage Mater.* **2021**, *35*, 334.
- [19] H. Shi, X. Ren, J. Lu, C. Dong, J. Liu, Q. Yang, J. Chen, Z. S. Wu, *Adv. Energy Mater.* **2020**, *10*, 2002271.
- [20] H. Zhang, X. Liao, Y. Guan, Y. Xiang, M. Li, W. Zhang, X. Zhu, H. Ming, L. Lu, J. Qiu, Y. Huang, G. Cao, Y. Yang, L. Mai, Y. Zhao, H. Zhang, *Nat. Commun.* **2018**, *9*, 3729.
- [21] X. Lan, W. Ye, H. Zheng, Y. Cheng, Q. Zhang, D. L. Peng, M. S. Wang, *Nano Energy* **2019**, *66*, 104178.
- [22] J. Sun, Y. Cheng, H. Zhang, X. Yan, Z. Sun, W. Ye, W. Li, M. Zhang, H. Gao, J. Han, D. L. Peng, Y. Yang, M. S. Wang, *Nano Lett.* **2022**, *22*, 5874.
- [23] C. Yu, Y. Du, R. He, Y. Ma, Z. Liu, X. Li, W. Luo, L. Zhou, L. Mai, *ACS Appl. Energy Mater.* **2021**, *4*, 3905.
- [24] L. Liu, Y. X. Yin, J. Y. Li, N. W. Li, X. X. Zeng, H. Ye, Y. G. Guo, L. J. Wan, *Joule* **2017**, *1*, 563.
- [25] C. Niu, H. Pan, W. Xu, J. Xiao, J. G. Zhang, L. Luo, C. Wang, D. Mei, J. Meng, X. Wang, Z. Liu, L. Mai, J. Liu, *Nat. Nanotechnol.* **2019**, *14*, 594.
- [26] W. Ye, F. Pei, X. Lan, Y. Cheng, X. Fang, Q. Zhang, N. Zheng, D. L. Peng, M. S. Wang, *Adv. Energy Mater.* **2020**, *10*, 1902956.
- [27] K. Yan, Z. Lu, H. W. Lee, F. Xiong, P. C. Hsu, Y. Li, J. Zhao, S. Chu, Y. Cui, *Nat. Energy* **2016**, *1*, 16010.
- [28] Y. Son, T. Lee, B. Wen, J. Ma, C. Jo, Y. G. Cho, A. Boies, J. Cho, M. De Volder, *Energy Environ. Sci.* **2020**, *13*, 3723.
- [29] Y. Zhang, G. Hu, Q. Yu, Z. Liu, C. Yu, L. Wu, L. Zhou, L. Mai, *Mater. Chem. Front.* **2020**, *4*, 1656.
- [30] Z. Liu, Y. Zhao, R. He, W. Luo, J. Meng, Q. Yu, D. Zhao, L. Zhou, L. Mai, *Energy Storage Mater.* **2019**, *19*, 299.
- [31] Q. Yu, P. Ge, Z. Liu, M. Xu, W. Yang, L. Zhou, D. Zhao, L. Mai, *J. Mater. Chem. A* **2018**, *6*, 14903.
- [32] Z. Liu, Q. Yu, Y. Zhao, R. He, M. Xu, S. Feng, S. Li, L. Zhou, L. Mai, *Chem. Soc. Rev.* **2019**, *48*, 285.
- [33] W. Luo, F. Li, J. J. Gaumet, P. Magri, S. Diliberto, L. Zhou, L. Mai, *Adv. Energy Mater.* **2018**, *8*, 1703237.
- [34] T. Wang, P. Zhai, D. Legut, L. Wang, X. Liu, B. Li, C. Dong, Y. Fan, Y. Gong, Q. Zhang, *Adv. Energy Mater.* **2019**, *9*, 1804000.
- [35] X. Chen, X. R. Chen, T. Z. Hou, B. Q. Li, X. B. Cheng, R. Zhang, Q. Zhang, *Sci. Adv.* **2019**, *5*, eaau7728.
- [36] W. Ye, F. Pei, X. Lan, Y. Cheng, X. Fang, Q. Zhang, N. Zheng, D. L. Peng, M. S. Wang, *Adv. Energy Mater.* **2020**, *10*, 1902956.
- [37] J. H. Um, S. H. Yu, *Adv. Energy Mater.* **2021**, *11*, 2003004.
- [38] N. Liu, H. Wu, M. T. McDowell, Y. Yao, C. Wang, Y. Cui, *Nano Lett.* **2012**, *12*, 3315.
- [39] T. T. Zuo, Y. X. Yin, S. H. Wang, P. F. Wang, X. Yang, J. Liu, C. P. Yang, Y. G. Guo, *Nano Lett.* **2018**, *18*, 297.
- [40] Y. Liu, D. Lin, Z. Liang, J. Zhao, K. Yan, Y. Cui, *Nat. Commun.* **2016**, *7*, 10992.
- [41] J. Xie, J. Wang, R. L. Hye, K. Yan, Y. Li, F. Shi, W. Huang, A. Pei, G. Chen, R. Subbaraman, J. Christensen, Y. Cui, *Sci. Adv.* **2018**, *4*, eaat5168.
- [42] S. Zhang, G. Yang, Z. Liu, S. Weng, X. Li, X. Wang, Y. Gao, Z. Wang, L. Chen, *ACS Energy Lett.* **2021**, *6*, 4118.